EJNMMI Research

ORIGINAL RESEARCH

Open Access

Association of white matter injury and neuroinflammation in the post-acute phase after ischemic stroke using [^{18}F]FEPPA-PET/MRI

Stefan E. Poirier[1,2*], Rachel Wagner[3], Linshan Liu[1], Pavlo Ohorodnyk[4], Michael T. Jurkiewicz[4], Alexander Thiel[5], Jonathan D. Thiessen[1,2,4,6,7], Alexander V. Khaw[1,8†] and Udunna C. Anazodo[1,2,8,9*†]

Abstract

Background Cerebral white matter (WM) injury after ischemic stroke is associated with post-stroke cognitive impairment (PSCI), however, the interaction between sustained neuroinflammation and post-stroke WM injury is not well understood. Hybrid PET/MRI can provide insight into pathophysiological mechanisms linking chronic neuroinflammation, ischemic WM injury, and PSCI. Using PET/MRI, this study investigated the relationship between [^{18}F]FEPPA standardized uptake value ratio (SUVr) measurements of glial activation and diffusion tensor imaging (DTI) measurements of microstructure integrity in brain WM regions in the chronic phase at 6-months after acute ischemic stroke.

Results [^{18}F]FEPPA-PET, DTI, and T2-weighted FLAIR were acquired at 6-months post-stroke in 19 elderly humans (seven females; mean age = 76 ± 5 years) with confirmed first-ever acute ischemic stroke using hybrid PET/3T-MRI. Index infarcts, chronic (incidental, covert) infarcts, and WM hyperintensities were manually segmented on FLAIR and excluded from the imaging analysis. Pearson correlation was conducted to assess the association between [^{18}F]FEPPA-SUVr and DTI measurements in WM regions commonly implicated in PSCI. [^{18}F]FEPPA-SUVr was elevated in brain regions ipsilateral to the index infarct at 6-months post-stroke, and these increases correlated with decreases in fractional anisotropy in several WM pathways linked to PSCI, including right superior longitudinal fasciculus (SLF) III (r = -0.82, p < 0.0001), right anterior thalamic radiation (r = -0.61, p = 0.006), and right arcuate fasciculus (r = -0.56, p = 0.01). Elevated [^{18}F]FEPPA-SUVr was also associated with increased mean diffusivity (r = 0.69, p < 0.001), axial diffusivity (r = 0.55, p = 0.02), and radial diffusivity (r = 0.74, p < 0.001) in right SLF III.

†Alexander V. Khaw and Udunna C. Anazodo contributed equally to this work.

*Correspondence:
Stefan E. Poirier
spoirie6@uwo.ca
Udunna C. Anazodo
udunna.anazodo@mcgill.ca

Full list of author information is available at the end of the article

Conclusions This study found an association between elevated post-acute glial activation (neuroinflammation) and reduced microstructure integrity in brain WM pathways ipsilateral to ischemic infarcts and remote from WM lesions at 6-months post-stroke. Hybrid PET/MRI is promising to be a valuable tool for probing post-acute neuroinflammation and associated changes in cerebral WM pathways following ischemic stroke.

Keywords PET/MRI, [^{18}F]FEPPA, Stroke, Neuroinflammation, White matter, Diffusion tensor imaging

Introduction

In elderly humans, cerebral white matter (WM) injury after acute ischemic stroke is common and associated with post-stroke cognitive impairment and decreased quality of life [1]. Post-stroke WM damage can occur both within immediate projections from and to the acute brain infarct area, as well as in remote brain tissue [2, 3]. Neuroimaging can visualize and characterize ischemic brain lesions as well as detect changes in cerebral WM structure and function following stroke [4]. WM hyperintensities (WMHs), or leukoaraiosis, are frequently observed on T2-weighted fluid attenuated inversion recovery (FLAIR) MRI images in brains of stroke patients, as well as healthy elderly adults [1, 4]. However, post-acute changes to the underlying microstructure of normal appearing WM (NAWM) and its relationship to ischemic brain lesions in the months following stroke remain less explored. One longitudinal MRI study using diffusion tensor imaging (DTI) and FLAIR to assess NAWM microstructure and WMH progression in elderly adults at risk for stroke showed that decreases in fractional anisotropy (FA), increases in mean diffusivity (MD), and elevations in FLAIR signal in NAWM predict conversion of NAWM into WMHs within 3.5 years of follow-up [5]. Similarly, another diffusion MRI study recently found widespread breakdown of WM structural integrity in elderly patients within 3-years post-stroke [6]. Thus, multimodal brain imaging can assess post-acute changes in cerebral WM structure following stroke and may provide a better understanding of the associations between cerebrovascular injury, secondary NAWM damage remote from infarction, and post-stroke cognitive outcomes.

Ischemic WM injury and post-acute degeneration of remote NAWM following stroke may be mediated by sustained neuroinflammation [7, 8]. However, the pathophysiological mechanisms linking chronic extralesional neuroinflammation, remote WM injury, and post-stroke cognitive impairment are not well understood. Ischemic stroke onset has been shown to trigger neuroinflammation in the form of glial activation [9]. Previous studies on the trajectory of neuroinflammation in vascular and neurodegenerative diseases have shown glial activation to follow a biphasic pattern, with an initial acute reparative phase and a switch to a later, chronic pro-inflammatory phase [10, 11]. In some stroke patients, the pro-inflammatory phenotype can sustain chronically and may exacerbate neurodegenerative processes, including WM disease [7, 12].

Molecular imaging techniques, such as positron emission tomography (PET) are used to image brain tissue inflammation involved in response to ischemic WM injury. PET radioligands which target upregulation of translocator proteins (TSPO) highly expressed on activated brain glial cells (microglia and astrocytes) may provide a measurement of chronic WM inflammation after stroke [8]. Specifically, elevation in TSPO-PET standardized uptake value (SUV) is considered an imaging biomarker of neuroinflammation [13, 14]. Past studies have shown TSPO uptake to be elevated in brain regions implicated in several neurodegenerative diseases and neuropsychological disorders including Alzheimer's disease [15], Parkinson's disease [16], frontotemporal dementia [17], and major depressive disorder [18]. Second generation TSPO ligands, such as [^{18}F]FEPPA and [^{18}F]DPA-714, have increased affinity for TSPO relative to first generation TSPO-PET tracers [19, 20]. [^{18}F]FEPPA is an established TSPO-PET tracer for imaging glial activation [14, 21] and can be used to assess neuroinflammation after ischemic stroke [22].

Hybrid PET/MR imaging of the brain affords the opportunity to simultaneously probe molecular and structural changes in brain tissue following ischemic stroke. Because WM disease is closely associated with ischemic brain injury, multimodal imaging combining [^{18}F]FEPPA-PET and DTI could shed light into pathophysiological mechanisms linking chronic neuroinflammation remote from infarction, ischemic WM injury, and post-stroke cognitive impairment. In this study, hybrid [^{18}F]FEPPA-PET/MRI was used to investigate the relationship between [^{18}F]FEPPA-SUV measurements of elevated post-acute glial activation (as a biomarker of neuroinflammation) and DTI measurements of WM microstructure integrity in brains of elderly adults at 6-months following an acute ischemic stroke.

Materials and methods

Patients

Elderly adults with confirmed first-ever acute ischemic stroke were recruited from a comprehensive stroke centre (London Health Sciences Centre) to participate in this study. Upon hospital admission or evaluation in the Emergency Department for acute stroke symptoms, all patients underwent a standard-of-care diagnostic workup

within 24–48 h post-stroke to detect the infarct territory. The diagnostic workup included examination of patient medical history and acute clinical imaging (1.5T MRI and/or contrast-enhanced computed tomography (CT)) of the brain and blood-supplying arteries. Acute clinical 1.5T MRI included T2-weighted FLAIR and diffusion-weighted imaging (DWI) to detect structural abnormalities in the brain following ischemic stroke. Acute ischemic stroke was confirmed on brain imaging (1.5T MRI or CT) with an ischemic infarct that corresponded with the presenting neurologic deficit. Patients between 65 and 85 years of age who had an acute ischemic lesion with a minimum diameter of 5 mm were enrolled in the study. All patients were functionally independent in all basic and instrumental activities of daily living and had an average Informant Questionnaire on Cognitive Decline in the Elderly (IQCODE) score ≤ 3.44 (no significant decline in cognitive function over the past 10 years). Each patient's index stroke event occurred within 2-weeks prior to study enrollment with a clear, documented symptom onset or new wake-up symptoms attributable to the stroke. TSPO genotyping for the rs6971 polymorphism was performed using blood samples from patients. Exclusion criteria for this study included patients with: (1) stroke due to parenchymal hemorrhage; (2) history of a previous symptomatic stroke (covert infarcts detected incidentally on brain imaging were not an exclusion criterion); (3) presence of other neurological or psychiatric disease, such as dementia or mild cognitive impairment (MCI), prior to study entry; (4) significant aphasia limiting the comprehension or ability of patients to complete cognitive testing; (5) evidence of other chronic co-morbid conditions or unstable acute systemic illnesses which could shorten the patient's survival or limit their ability to complete the study; (6) contraindication to MRI; and (7) low-affinity TSPO binding to minimize large variability in [^{18}F]FEPPA binding as supported by a previous report finding that approximately 10% of Caucasians carry the allele for low-affinity TSPO binding [23]. All patients underwent a 6-month follow-up visit including neuropsychological evaluation, blood testing, and brain PET/MR imaging. During this follow-up visit, global cognitive function was assessed in patients using the Montreal Cognitive Assessment (MoCA; Version 7.1) [24] to evaluate post-acute cognitive performance following stroke. This study was approved by the Western University Research Ethics Board and written informed consent was obtained from all patients.

Data acquisition

This study consisted of brain scans acquired on all patients during the acute diagnostic workup and post-acute, 6-month follow-up visit. Acute clinical imaging was performed on patients within 2-days post-stroke using 1.5T MRI and/or CT, indicated based on the presenting acute stroke symptoms. All acute images were visually assessed by a stroke neurologist (A.V.K.) with over 25 years of clinical stroke imaging experience. The stroke neurologist measured the index infarct diameter on each patient's acute images using a clinical image viewer (Xero Viewer, Agfa Healthcare). Index infarcts had a minimum diameter of 5 mm and were detected as hyperintensity on DWI or hypodensity on CT.

To assess post-acute changes to the brain, imaging data were acquired on patients at 6-months post-stroke using a hybrid PET/3T-MRI scanner (Biograph mMR, Siemens Healthineers, Erlangen, Germany) with a 12-channel PET-compatible head coil. PET and MRI were acquired simultaneously immediately following an intravenous injection of 203 ± 22 MBq of [^{18}F]FEPPA. Dynamic [^{18}F]FEPPA-PET images were acquired in a 90-min list-mode imaging session during serial MRI scans. The MRI scans were: a high resolution T1-weighted MRI (1 mm^3 isotropic voxels) acquired using a three-dimensional (3D) magnetization-prepared rapid gradient-echo (MPRAGE) sequence, a 3D T2-weighted FLAIR (1 mm^3 isotropic voxels), and a two-dimensional (2D) single-shot echo-planar imaging (EPI) DWI scan acquired using the following parameters: 30 diffusion-encoding directions; b-values = 0 and 1000 s/mm^2; 2 mm^3 isotropic voxels; and two b0 images acquired in opposite phase-encoding directions to correct for inherent susceptibility-induced distortions in DWI. The list-mode [^{18}F]FEPPA-PET data acquired at 60–90 min post-injection were reconstructed into six 5-min frames using Siemens e7 tools and an iterative algorithm (ordered subset expectation maximization; 3 iterations, 21 subsets, 3D Gaussian filter with a full-width at half-maximum of 2 mm, 344 × 344 × 127 matrix with 1.04 × 1.04 × 2.03 mm^3 voxel size, and zoom factor of 2). The PET reconstruction included corrections for scatter, decay, and dead time while attenuation correction was performed using an MR-based approach [25].

3T FLAIR image reading and lesion segmentation at 6-months post-stroke

3T FLAIR was used to detect and manually segment structural brain lesions in patients at 6-months following ischemic stroke. Prior to image reading, each patient's 3T FLAIR image was preprocessed to improve spatial alignment of FLAIR to anatomical T1-weighted MRI. FLAIR preprocessing steps were completed using Statistical Parametric Mapping (SPM12) (Wellcome Department of Cognitive Neurology, Institute of Neurology, London), MATLAB R2022a (MathWorks®, Natick, MA), and Functional MRI of the Brain Software Library (FSL) [26]. Each patient's FLAIR image was first rigidly aligned to their structural T1-weighted image at 6-months post-stroke

using the *Coregister: Estimate & Reslice* module in SPM12. A whole-brain mask– generated from automated tissue segmentation of each patient's T1-weighted image using the segmentation module in Computational Anatomy Toolbox (CAT12) [27]– was then applied to remove extracerebral voxels from the FLAIR image.

Each patient's preprocessed 3T FLAIR image at 6-months post-stroke was visually assessed by a stroke neurologist (A.V.K.) with over 25 years of clinical stroke imaging experience and in consultation with two neuroradiologists (P.O. and M.T.J.). The stroke neurologist and neuroradiologists were aware of all clinical information while visually reading the 3T FLAIR images. Visual assessment and manual segmentation of 3T FLAIR images were completed using ITK-SNAP [28] (http://www.itksnap.org/; Version 4.0.2). Specifically, each patient's 3T FLAIR image was visually inspected for evidence of three types of cerebrovascular-related lesions: (1) WMHs; (2) index infarcts; and (3) chronic (covert) infarcts. Briefly, regarding the classification of lesion type, WMHs were considered as evidence of WM disease remote from brain infarction. Index infarcts were identified as the infarct responsible for the acute presentation with stroke symptoms, determined based on all available clinical information. Chronic infarcts were detected incidentally as covert or silent infarcts on brain imaging after stroke. A binary label map was created for each patient by manually segmenting WMHs, index infarcts, and chronic infarcts along contiguous slices of each patient's 3T FLAIR image at 6-months post-stroke using the polygon and paintbrush tools in ITK-SNAP. Binary segmentation masks of each lesion type (WMHs, index infarcts, chronic infarcts) were extracted from each patient's binary label map using the *fslmaths* command in FSL. To ensure fair voxel-wise comparison of lesions across patient brains, each patient's post-acute 3T FLAIR image and manual lesion segmentation masks were spatially normalized to a Montreal Neurological Institute (MNI) T1 1-mm brain template provided by FSL using a 3-step image registration algorithm (consisting of rigid, affine, and deformable transformations) in Advanced Normalization Tools (ANTs) [29]. Finally, to quantify the extent of post-acute cerebrovascular injury at 6-months post-stroke, the volumes of each lesion type were calculated as the sum of all voxels in each patient's manual lesion segmentation masks using MATLAB.

Preprocessing of [^{18}F]FEPPA-PET data at 6-months post-stroke

[^{18}F]FEPPA-PET images at 6-months post-stroke were preprocessed using SPM12 and ANTs. To correct for subject motion, all [^{18}F]FEPPA-PET images were aligned to the first time frame using the *Realign* module in SPM12. Each patient's [^{18}F]FEPPA-PET image was converted to an SUV map using net injected dose of [^{18}F]FEPPA and body weight. To ensure fair voxel-wise comparison across patient brains, each patient's post-acute SUV map was spatially normalized to an MNI T1 1-mm brain template provided by FSL using a 3-step image registration algorithm (consisting of rigid, affine, and deformable transformations) in ANTs. To account for global metabolism effects in the brain, each patient's SUV map was then normalized using the cerebellum as a pseudo-reference region [30] to generate an SUV ratio (SUVr) map for quantification of brain [^{18}F]FEPPA-PET signal (TSPO uptake) in the post-acute phase at 6-months following stroke.

Regional analysis of the relationship between [^{18}F]FEPPA-SUVr and DTI metrics in normal appearing white matter at 6-months post-stroke

A lesion-exclusion approach was used to relate [^{18}F]FEPPA-PET measurements of post-acute glial activation (neuroinflammatory load) to DTI parameters of microstructural integrity in NAWM regions at 6-months following ischemic stroke. Preprocessing and tensor-fitting of each patient's DWI data at 6-months post-stroke were performed as previously described [31] to generate FA, MD, axial diffusivity (AD), and radial diffusivity (RD) maps. Using each patient's preprocessed DWI images, WM bundles were automatically segmented using TractSeg [32] as previously described [33]. Specifically, the imaging analysis was focused on nine WM bundles commonly implicated in post-stroke cognitive impairment [6]: left/right arcuate fasciculus (AF), left/right anterior thalamic radiation (ATR), rostrum of corpus callosum (CC), anterior midbody of CC, splenium of CC, and left/right superior longitudinal fasciculus (SLF) III. To ensure fair voxel-wise comparison across patient brains, all post-acute diffusion MRI data (DTI parameter maps, WM bundle segmentations) were spatially normalized to an MNI T1 1-mm brain template provided by FSL using a 3-step image registration algorithm (consisting of rigid, affine, and deformable transformations) in ANTs. Exclusion masks of WMHs, index infarcts, and chronic infarcts (derived from manual segmentation of lesions on 3T FLAIR at 6-months post-stroke) were applied to remove lesioned voxels from each patient's WM bundles and generate NAWM bundle segmentation masks. Additionally, a whole-brain WM mask (derived from tissue segmentation of structural T1-weighted MRI at 6-months post-stroke) was also applied to each patient's NAWM bundle segmentation masks to minimize partial volume effects from non-WM signal (gray matter, cerebrospinal fluid) on the regional NAWM analysis. Mean [^{18}F]FEPPA-SUVr (relative to cerebellum), FA, MD, AD, and RD values were calculated in each patient's NAWM bundles using MATLAB. Pearson correlation was conducted to assess

the association between [^{18}F]FEPPA-SUVr and DTI measurements (FA, MD, AD, RD) in each NAWM bundle across all patients at 6-months post-stroke. To provide a preliminary evaluation of the relationship between post-acute WM changes and global cognitive performance, Spearman rank correlation was used to assess the association between imaging biomarkers ([^{18}F]FEPPA-SUVr, FA, MD, AD, RD) in each NAWM bundle and MoCA across all patients at 6-months post-stroke. For all correlational analyses, $p < 0.05$ was considered statistically significant.

Results

Twenty-five elderly adults with acute ischemic stroke were initially enrolled in this study. Two patients carried the allele for low-affinity TSPO binding and were excluded from further study procedures. Four patients did not undergo PET/MRI scanning at 6-months post-stroke due to patient withdrawal and were excluded from analysis. Thus, this study had a final sample size of nineteen patients (seven females; mean age = 76 ± 5 years). Study demographics, baseline characteristics, and clinical findings at hospital admission including National Institutes of Health Stroke Scale (NIHSS) scores, and index infarct diameter and location are summarized in Table 1. Across all patients, the mean NIHSS score and index infarct diameter at onset of stroke were 5.8 ± 6.5 and 2.9 ± 2.2 cm, respectively. Acute clinical 1.5T MRI and CT within 2-days post-stroke was indicated in 15/19 (79%) patients and 17/19 (89%) patients, respectively. Acute clinical 1.5T MRI revealed structural brain abnormalities associated with cerebrovascular disease in the left hemisphere of 8/19 (42%) patients, right hemisphere of 5/19 (26%) patients, and bilateral hemispheres of 2/19 (11%) patients. Based on all available clinical information, the clinical diagnosis was confirmed to be left-sided ischemic stroke in 11/19 (58%) patients, right-sided ischemic stroke in 7/19 (37%) patients, and brain stem ischemic stroke in 1/19 (5%) patients. TSPO genotyping revealed that 13/19 (68%) patients were high-affinity binders and 6/19 (32%) patients were mixed-affinity binders.

Post-acute, qualitative [^{18}F]FEPPA-PET/3T-MRI findings from one representative stroke patient (patient #1) at 6-months following stroke are provided in Fig. 1.

Table 1 Study demographics, baseline characteristics, and clinical findings at hospital admission

Patient #	Sex	Age (yr)	Cardiovascular Risk Factors	NIHSS	Index Infarct Diameter (cm)	Index Infarct Location	Chronic Infarcts	TSPO Status
1	M	78	Alcohol use	2	8	L temp/L occ/L par	Y	HAB
2	M	70	HTN, AF, ex-smoker, alcohol use	1	2.8	L front/L occ	Y	HAB
3	M	69	HTN, AF, ex-smoker, alcohol use	21	4.6	L insula/L temp	N	MAB
4	M	78	Ex-smoker	0	3.72	L par	Y	MAB
5	M	80	HTN	9	1.72	Bitemporal/L occ/L par	Y	HAB
6	F	76	HTN	3	1	R par	N	MAB
7	M	75	HTN, DM, ex-smoker	8	1.3	Left MCA	N	HAB
8	M	82	HTN, DLP, alcohol use	4	0.7	L insula/L front/L thalamus	Y	HAB
9	M	76	HTN, DLP	1	1.3	L front/L thalamus	N	MAB
10	F	80	HTN, DLP, CAD, PAD	2	7	Bifrontal/R temp	N	HAB
11	F	66	HTN, smoker, alcohol use	2	1.6	L cerebellum/Brain stem	Y	HAB
12	M	72	HTN, DLP, ex-smoker, alcohol use	6	4.5	L insula/L par	Y	HAB
13	F	84	DLP, alcohol use	2	2	R par	N	MAB
14	M	74	HTN, DLP, ex-smoker, alcohol use	7	1.8	R cerebellum	N	HAB
15	M	78	HTN, DLP, DM, CAD, ex-smoker, alcohol use	1	5.8	L cerebellum	N	MAB
16	M	74	HTN, DLP, AF, smoker, alcohol use	7	0.68	Left MCA	Y	HAB
17	F	82	HTN, DLP, depression, ex-smoker, alcohol use	21	1.98	Left MCA	N	HAB
18	F	77	HTN, DLP, PAD, alcohol use	0	0.77	R caudate/R corona radiata	Y	HAB
19	F	81	HTN, DLP, AF, DM, CAD, depression, ex-smoker, alcohol use	14	4.3	Right MCA	Y	HAB

Note. NIHSS and index infarct diameter were assessed at time of index stroke event. Index infarct location was determined based on reports from acute clinically indicated 1.5T MRI (FLAIR, DWI) and CT within 2-days post-stroke as well as clinical notes at hospital admission

Abbreviations: AF, atrial fibrillation; CAD, coronary artery disease; DLP, dyslipidemia; DM, diabetes mellitus; front, frontal lobe; F, female; HAB, high-affinity binder; HTN, hypertension; L, left; M, male; MAB, mixed-affinity binder; MCA, middle cerebral artery; NIHSS, National Institutes of Health Stroke Scale; N, no; occ, occipital lobe; PAD, peripheral arterial disease; par, parietal lobe; R, right; temp, temporal lobe; Y, yes

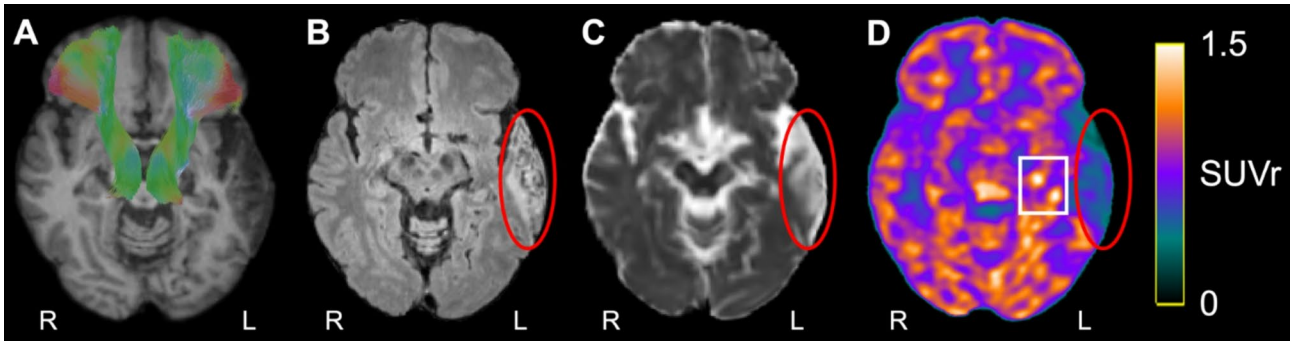

Fig. 1 Brain PET/3T-MR images from a 78-year-old male stroke patient (patient #1) at 6-months post-stroke: **(A)** white matter tractography using TractSeg shows right and left anterior thalamic radiation bundles (coloured lines) overlaid onto T1-weighted MRI; **(B)** T2-weighted FLAIR shows index infarct (red circle); **(C)** apparent diffusion coefficient (ADC) map shows elevated ADC within index infarct (red circle); and **(D)** [^{18}F]FEPPA-SUVr map shows elevated [^{18}F]FEPPA uptake (white rectangle) ipsilateral to index infarct (red circle) and decreased [^{18}F]FEPPA uptake within index infarct compared to contralateral hemisphere

Table 2 Patient characteristics, bloodwork results, MoCA scores, and quantitative lesion findings at 6-months post-stroke

Variable	Result	Variable	Result
Age (yr)	76 ± 5 (66–84, *n* = 19)	Resting heart rate (beats per min)	69.0 ± 11.3 (51–87, *n* = 14)
Females (%)	36.8 (*n* = 19)	Total cholesterol (mmol/L)	3.42 ± 0.31 (2.75–3.69, *n* = 9)
Hypertension (%)	84.2 (*n* = 19)	HDL (mmol/L)	1.40 ± 0.40 (0.90–2.05, *n* = 9)
Dyslipidemia (%)	57.9 (*n* = 19)	LDL (mmol/L)	1.41 ± 0.23 (1.14–1.74, *n* = 9)
Atrial fibrillation (%)	21.1 (*n* = 19)	Non-HDL cholesterol (mmol/L)	2.02 ± 0.30 (1.64–2.58, *n* = 9)
Diabetes mellitus (%)	15.8 (*n* = 19)	Triglycerides (mmol/L)	1.42 ± 0.49 (1.06–2.62, *n* = 9)
CKD (%)	0 (*n* = 19)	Fasting blood glucose (mmol/L)	7.13 ± 2.19 (5.00–12.3, *n* = 10)
CAD (%)	15.8 (*n* = 19)	HbA1c (%)	5.81 ± 0.38 (5.20–6.20, *n* = 8)
CHF (%)	0 (*n* = 19)	CRP (mg/L)	5.45 ± 7.50 (0.60–19.4, *n* = 11)
PAD (%)	10.5 (*n* = 19)	ESR (mm/hr)	18.0 ± 13.6 (2–40, *n* = 8)
Depression (%)	10.5 (*n* = 19)	MoCA	26.0 ± 1.97 (23–30, *n* = 19)
Smoker (%, current/ex/never)	10.5/47.4/42.1 (*n* = 19)	WMH volume (cm^3)	17.0 ± 27.9 (0.15–113.3, *n* = 19)
Alcohol use (%)	68.4 (*n* = 19)	Index infarct volume (cm^3)	8.00 ± 12.1 (0.11–48.5, *n* = 19)
Rest supine systolic BP (mmHg)	136.9 ± 14.3 (107–161, *n* = 15)	Chronic infarct volume (cm^3)	3.29 ± 5.15 (0.62–17.3, *n* = 10)
Rest supine diastolic BP (mmHg)	74.6 ± 6.98 (63–86, *n* = 14)	Chronic infarcts (%)	52.6 (*n* = 19)

Note. Results are reported as mean ± standard deviation (min–max, sample size n)

Abbreviations: BP, blood pressure; CAD, coronary artery disease; CHF, congestive heart failure; CKD, chronic kidney disease; CRP, C-reactive protein; ESR, erythrocyte sedimentation rate; HDL, high-density lipoprotein; LDL, low-density lipoprotein; MoCA, Montreal Cognitive Assessment; PAD, peripheral arterial disease

Figure 1A shows WM bundles for patient #1 visualized using TractSeg. In this patient, visual assessment of post-acute 3T FLAIR revealed the index infarct in the chronic stage in the left temporal lobe (Fig. 1B) and a chronic, covert infarct in the left occipital lobe. Similarly, this patient's post-acute DTI parameter maps showed reduced FA as well as elevated apparent diffusion coefficients (Fig. 1C), MD, AD, and RD within the index infarct. Visual assessment of this patient's post-acute [^{18}F]FEPPA-SUVr map revealed elevated [^{18}F]FEPPA uptake in brain areas ipsilateral to the index infarct and decreased [^{18}F]FEPPA uptake within the index infarct compared to the contralateral hemisphere (Fig. 1D).

Bloodwork results and MoCA scores from the 6-month follow-up visit are summarized in Table 2. Across all patients, the mean MoCA score was 26.0 ± 1.97 (23–30). Specifically, 9/19 (47%) patients had MoCA score ≥ 26 (cognitively healthy), while 10/19 (53%) patients had MoCA score between 23 and 25 (potential MCI). Manual segmentation of cerebrovascular-related lesions on 3T FLAIR at 6-months post-stroke revealed heterogeneous spatial distribution of WMHs, index infarcts, and chronic infarcts across all patient brains, as illustrated in five representative patients (patients #1, #3, #8, #13, and #16) in Fig. 2. Specifically, WMHs, index infarcts, and chronic infarcts were detected on 3T FLAIR in 19/19 (100%) patients, 19/19 (100%) patients, and 10/19 (53%) patients, respectively. Index infarcts in the chronic stage were found in the left hemisphere of 12/19 (63%) patients, right hemisphere of 5/19 (26%) patients, and bilateral hemispheres of 2/19 (11%) patients. Chronic infarcts were detected in the left hemisphere of 4/19 (21%) patients, right hemisphere of 1/19 (5%) patients, and bilateral hemispheres of 5/19 (26%) patients. Across

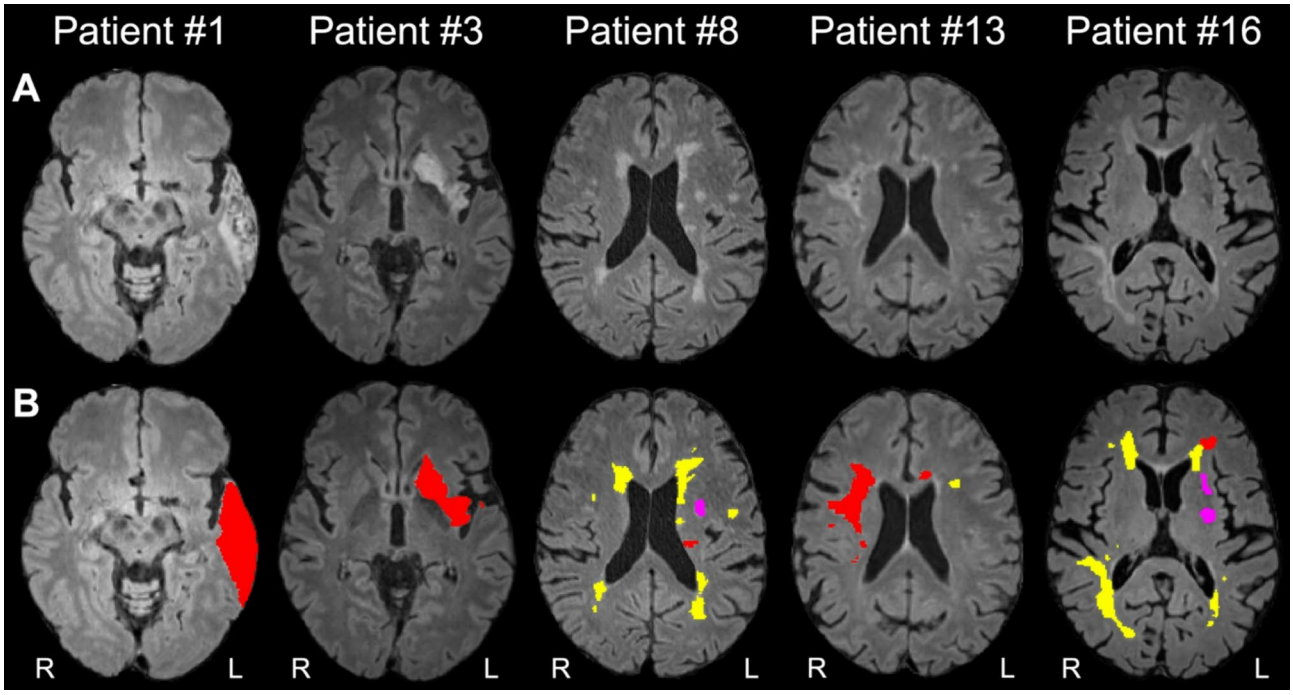

Fig. 2 **(A)** T2-weighted FLAIR MRI image from five representative stroke patients (patient #1: 78-year-old male; patient #3: 69-year-old male; patient #8: 82-year-old male; patient #13: 84-year-old female; patient #16: 74-year-old male) at 6-months following stroke. **(B)** Manual segmentations of WM hyperintensities (yellow), index infarcts (red), and chronic infarcts (magenta) are shown overlaid onto FLAIR image. Index infarcts are identified as the infarct responsible for hospital admission (acute ischemic stroke). In patients #8 and #16, chronic infarcts are detected incidentally on FLAIR as covert or silent brain infarcts

all patients, the mean volume of WMHs, index infarcts, and chronic infarcts at 6-months post-stroke was 17.0 ± 27.9 (0.15–113.3) cm^3, 8.00 ± 12.1 (0.11–48.5) cm^3, and 3.29 ± 5.15 (0.62–17.3) cm^3, respectively.

Pearson correlation revealed significant associations between [^{18}F]FEPPA-SUVr and DTI measurements in several NAWM pathways linked to post-stroke cognitive impairment at 6-months following stroke (Fig. 3). Pearson correlation values for each NAWM bundle are summarized in Table 3. Across all patients, increases in [^{18}F]FEPPA-SUVr were significantly correlated with decreases in FA in right SLF III (r = -0.82, $p < 0.0001$), right ATR (r = -0.61, $p = 0.006$), right AF (r = -0.56, $p = 0.01$), left AF (r = -0.52, $p = 0.02$), left ATR (r = -0.46, $p = 0.049$), and rostrum of CC (r = -0.46, $p = 0.047$). Elevations in [^{18}F]FEPPA-SUVr were associated with increases in MD ($r = 0.69$, $p < 0.001$), increases in AD ($r = 0.55$, $p = 0.02$), and increases in RD ($r = 0.74$, $p < 0.001$) in right SLF III. Increases in [^{18}F]FEPPA-SUVr were also correlated with increases in MD ($r = 0.49$, $p = 0.03$) and increases in RD ($r = 0.54$, $p = 0.02$) in right AF, as well as increases in MD ($r = 0.50$, $p = 0.03$) and increases in RD ($r = 0.53$, $p = 0.02$) in right ATR. No significant associations were found between [^{18}F]FEPPA-SUVr and any of the DTI parameters in anterior midbody of CC or splenium of CC. Similarly, across all patients, Spearman rank correlation revealed no significant associations between imaging biomarkers ([^{18}F]FEPPA-SUVr, FA, MD, AD, RD) in any of the NAWM bundles and MoCA at 6-months post-stroke.

Discussion

This study used hybrid [^{18}F]FEPPA-PET/MRI to assess post-acute changes in WM related to cerebrovascular injury in brains of elderly adults at 6-months following an acute ischemic stroke. Here, a lesion-exclusion based imaging approach was applied combining [^{18}F]FEPPA-PET, DTI, and FLAIR to investigate the relationship between [^{18}F]FEPPA-SUV measurements of post-acute glial activation and DTI measurements of microstructural integrity in regional NAWM pathways remote from cerebrovascular-related lesions (WMHs, infarcts). Using this lesion-exclusion approach, elevations in post-acute glial activation were found to be associated with reductions in microstructural integrity in NAWM regions ipsilateral to ischemic infarcts and remote from WM lesions at 6-months post-stroke. These findings suggest that in some patients, [^{18}F]FEPPA-PET can show elevations in [^{18}F]FEPPA uptake (glial activation associated with chronic neuroinflammation) in NAWM in the chronic stage, months after an acute ischemic stroke. Thus, this study provides preliminary evidence that hybrid [^{18}F]FEPPA-PET/MRI may be a valuable multimodal brain imaging tool for simultaneously relating functional and

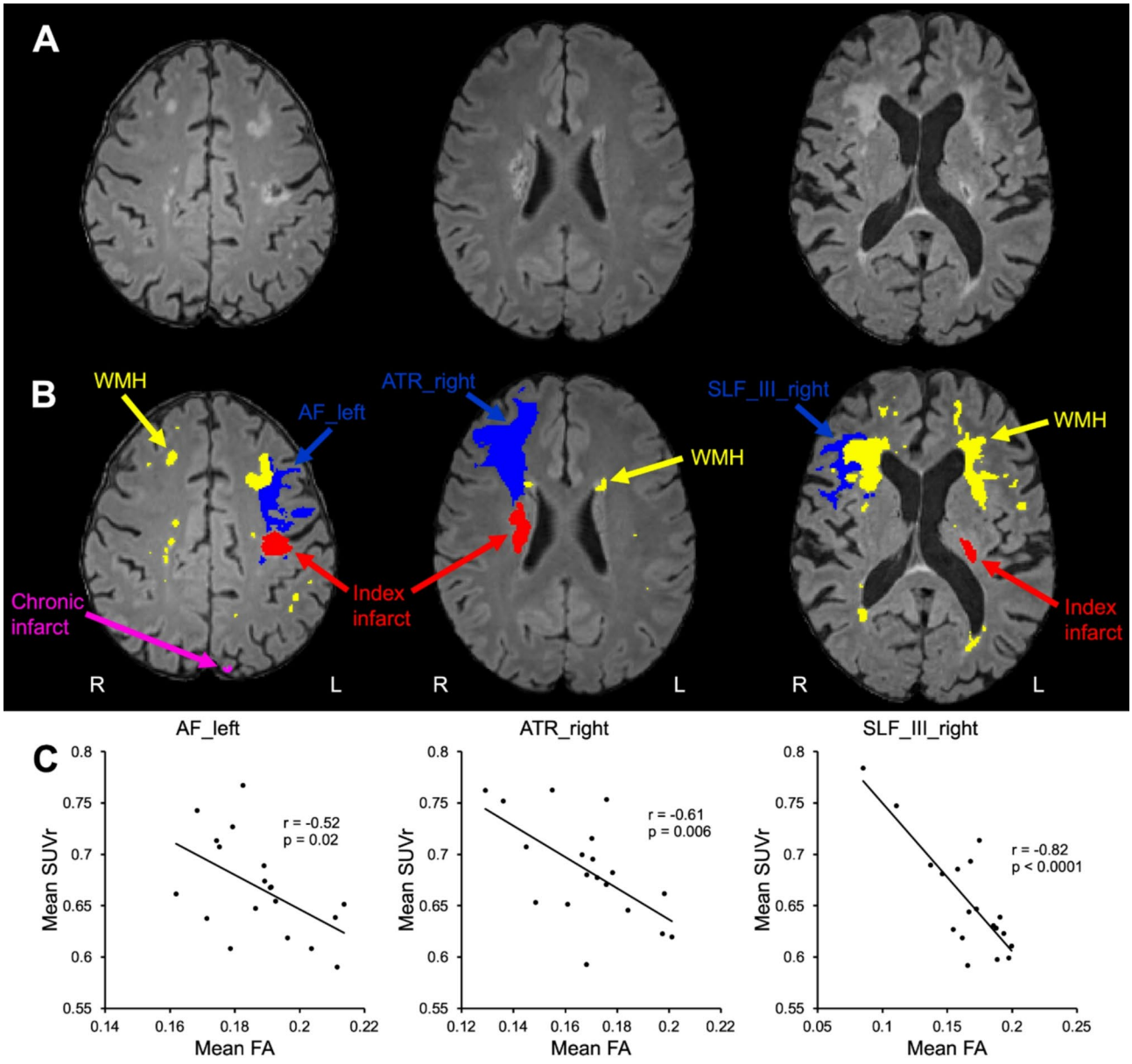

Fig. 3 **(A)** T2-weighted FLAIR at 6-months post-stroke and **(B)** visual representation of lesion exclusion approach overlaid onto FLAIR shows index infarcts (red), chronic infarcts (magenta), and WM hyperintensities (yellow) adjacent to normal appearing WM bundle segmentations (blue) for *a priori* WM regions implicated in stroke; left AF in a 70-year-old male stroke patient (patient #2), right ATR in a 76-year-old female stroke patient (patient #6), and right SLF III in a 76-year-old male stroke patient (patient #9). **(C)** Pearson correlational plots show a negative association between [^{18}F]FEPPA-SUVr and FA in each WM bundle across all nineteen stroke patients at 6-months post-stroke

structural changes in brain WM linked to post-stroke cognitive impairment in the months following an acute ischemic stroke.

Cerebral WM damage secondary to vascular-related ischemic injury can occur following stroke [1]. Furthermore, poor cognitive outcomes after ischemic stroke are correlated with severity of WM injury [1, 34]. To date, most WM imaging studies in stroke have focused on assessing structural WM changes in the early (hyperacute, acute) phases of stroke [35, 36] with less known about longer-term (post-acute) WM changes and associations to post-stroke cognitive impairment. (Feng et al. 2015) used lesion mapping of stroke DWI data and found increased lesion load in the corticospinal tract during the acute phase of stroke to be a predictor of poor motor outcomes and limited clinical recovery at 3-months following stroke [35]. Likewise, a DTI study by (Puig et al. 2013) found decreases in FA in the corticospinal tract of the stroke-affected (ipsilateral) hemisphere at 30-days after middle cerebral artery stroke to also be a predictor

Table 3 Regional Pearson correlations between DTI and [^{18}F]FEPPA-SUVr in normal appearing white matter of patients ($n = 19$) at 6-months post-stroke

	AF_left	AF_right	ATR_left	ATR_right	CC_ros	CC_ant_mid	CC_splen	SLF_III_left	SLF_III_right
FA to SUVr Pearson r (p-value)	-0.52 (0.02)*	-0.56 (0.01)*	-0.46 (0.049)*	-0.61 (0.0057)*	-0.46 (0.047)*	-0.07 (0.77)	-0.26 (0.29)	-0.54 (0.02)*	-0.82 (0.00002)**
MD to SUVr Pearson r (p-value)	0.12 (0.63)	0.49 (0.03)*	0.21 (0.38)	0.50 (0.03)*	-0.17 (0.47)	-0.10 (0.69)	0.10 (0.67)	0.07 (0.79)	0.69 (0.00098)**
AD to SUVr Pearson r (p-value)	-0.03 (0.91)	0.37 (0.12)	0.10 (0.67)	0.41 (0.08)	-0.40 (0.09)	-0.16 (0.52)	0.04 (0.88)	-0.12 (0.63)	0.55 (0.015)*
RD to SUVr Pearson r (p-value)	0.21 (0.38)	0.54 (0.02)*	0.26 (0.28)	0.53 (0.02)*	-0.05 (0.84)	-0.07 (0.78)	0.13 (0.59)	0.19 (0.45)	0.74 (0.0003)**

Note. In each patient, the stroke infarct(s) and WM hyperintensities were excluded from the WM imaging analysis to generate normal appearing WM regions

Abbreviations: AF, arcuate fasciculus; ATR, anterior thalamic radiation; CC_ros, rostrum of corpus callosum; CC_ant_mid, anterior midbody (primary motor) of corpus callosum; CC_splen, splenium of corpus callosum; SLF_III, superior longitudinal fasciculus III

*Statistically significant correlation at $p < 0.05$ (uncorrected)

**Statistical significance survives region-wise correction for multiple comparisons ($\alpha_{Bonferroni} = 0.0056$)

of long-term motor deficits [36]. Similar to this study, a couple of other studies have also assessed longer-term (post-acute) changes in DTI parameters in cerebral WM pathways in the months following ischemic stroke [3, 6]. (Egorova-Brumley et al. 2023) used diffusion MRI to assess longitudinal changes in WM macrostructure and microstructure in elderly adults from 3-months up to 3-years post-stroke and found evidence of decline in WM structural integrity (decreased fiber cross-section, decreased fiber density) in several WM tracts, including the SLF, ATR, and CC in patients within 3-years post-stroke compared to healthy controls [6]. Another study by (Kancheva et al. 2022) conducted an inter-hemispheric comparison of DTI metrics in stroke-affected WM fibers and observed decreases in FA and increases in RD along damaged WM tracts connected to lesions in the ipsilateral hemisphere of patients within 7-months post-stroke [3]. Specifically, DTI biomarkers of WM microstructural breakdown (decreased FA, increased MD, increased AD, increased RD) are considered to reflect progressive manifestation of Wallerian degeneration in the months following ischemic stroke [37]. Although the DTI findings from this pilot study may have been impacted by lack of comparison with longitudinal changes in a healthy control group, the utility of DTI in probing post-acute changes in WM microstructure after ischemic stroke is evident. Future DTI studies using larger stroke cohorts and suitable healthy controls could provide further insight into post-acute WM microstructural alterations and potential influence on cognitive outcomes following ischemic stroke.

Cerebral WM degeneration following ischemic stroke may be exacerbated by neuroinflammation [7, 8, 12]. Ischemic stroke elicits a neuroinflammatory response involving the recruitment of glial cells (microglia and astrocytes), leukocytes, and peripheral immune cells to the site of cerebrovascular injury within the first few weeks after stroke [9, 38]. Past studies using TSPO-PET to image glial activation as a biomarker of post-stroke WM inflammation have observed elevated TSPO-PET signal in WM tissue proximal to infarcts within the acute phase of stroke in rodent models of focal cerebral ischemia [22] as well as in human stroke patients [39]. However, studies assessing whether chronic neuroinflammation is present, especially in remote WM regions, in human stroke patients are fewer. This study explored the use of a second-generation TSPO-PET radioligand, [^{18}F]FEPPA, in detecting post-acute glial activation as a measurement of chronic WM inflammation in elderly humans following ischemic stroke. One patient (patient #1) visually showed elevations in [^{18}F]FEPPA-SUVr ipsilateral to the index infarct as well as decreases in [^{18}F]FEPPA-SUVr within the index infarct compared to the contralateral hemisphere at 6-months post-stroke, suggesting a shift of activated brain glial cells from index infarct to remote brain tissue in the months after stroke. The relative contributions of microglial activation to TSPO-PET signal remains controversial. A study by (Owen et al. 2017) did not observe an increase in TSPO signal following pro-inflammatory activation of human brain microglia and suggested that elevated TSPO signal could reflect microglial density rather than microglial activation [40]. While future studies may be needed to fully elucidate the biological meaning of the TSPO signal in PET, this study supports the notion of a relationship linking elevations in post-acute glial activation– or density– to microstructural alterations in WM pathways remote from cerebrovascular injury.

This study found that post-acute elevations in [^{18}F]FEPPA-SUVr were associated with reductions in microstructural integrity (decreases in FA accompanied by increases in diffusivities) of brain WM pathways remote from infarcts and WMHs at 6-months post-stroke. Consistent with these findings, a previous pilot PET/MRI study observed concomitant increases in TSPO uptake measured with [^{11}C]PBR28 SUVr and changes in DTI

metrics (decreases in FA and increases in MD) in WM regions ipsilateral as well as contralateral to infarcts at 1-year after middle cerebral artery stroke in older patients compared to healthy controls [41]. Similarly, another study combining [^{11}C]PK11195 and diffusion tractography observed an *in vivo* relationship between remote microglial activation and disruptions in WM tracts connected to infarcts that evolved over a 6-month period following acute subcortical stroke [7]. These findings support multimodal brain imaging combining PET and MRI as a promising tool for relating neuroinflammatory loads and structural brain changes as well as tracking disease progression following ischemic stroke.

In this study, associations between elevations in [^{18}F]FEPPA-SUVr and decreases in FA were predominantly lateralized to right-sided WM bundles. One possibility is that these findings could reflect post-acute disruptions in unknown connections between ischemic brain lesions and remote WM pathways in the contralateral hemisphere of patients with left-sided acute ischemic stroke. A recent study using [^{123}I]CLINDE SPECT found elevated TSPO uptake (glial activation) in brain regions ipsilateral and contralateral to chronic infarcts in human stroke patients up to 128 days following middle cerebral artery stroke [42]. Similar to this study, past PET and MRI studies have also shown glial activation and structural changes in damaged WM tracts to occur both within the ischemic (ipsilateral) hemisphere as well as the non-ischemic (contralateral) hemisphere [3, 7, 41]. However, the exact reasons for lateralization of these WM findings are unknown and could be explored in future stroke research. Of note, a recent study using intradialytic DTI revealed changes in WM microstructure consistent with acute ischemic brain injury during hemodialysis in chronic kidney disease patients [43]. Nevertheless, future longitudinal PET/MRI studies with patients stratified based on severity of stroke and ischemic WM injury could be used to investigate lateralization and localization of post-acute WM changes, neuroinflammatory loads, and associations to post-stroke cognitive impairment over the months following stroke. Interestingly, changes in all four DTI parameters (decreased FA, increased MD, increased AD, increased RD) were significantly correlated with post-acute elevations in [^{18}F]FEPPA-SUVr in right SLF III. Past studies have shown neural networks connecting the SLF and AF to be associated with deficits in language processing [44] and visual neglect [45] following stroke, suggesting the SLF and AF may be important WM tracts implicated in post-stroke recovery and cognitive outcomes.

This study did not observe any significant associations between global cognitive performance and regional [^{18}F]FEPPA-SUVr or DTI measurements, likely owing to the narrow range of MoCA scores (range: 23–30). Although frequently used in early dementia screening, MoCA is considered a broad cognitive assessment tool and may be less sensitive to subtle changes in cognitive function associated with MCI [46], particularly following stroke [47]. It is quite possible that the MoCA test may not have detected cognitive impairment in impaired stroke patients, since it does not test for processing speed– a cognitive domain often affected following stroke [47]. As such, the findings from this study suggest that MoCA alone may be insufficient to determine whether chronic WM inflammation is a potentiator of post-stroke cognitive impairment. Perhaps the use of a more comprehensive neuropsychological test battery, such as NINDS-CSN [48] or Creyos [49] targeting specific cognitive domains (i.e., executive function, visuospatial processing, verbal memory) in a larger stroke cohort with a wider range of MoCA scores could provide a better assessment of the relationship between post-stroke WM changes and cognitive outcomes.

In addition to detecting functional and structural brain changes after ischemic cerebrovascular injury, neuroimaging could also be used to help identify imaging biomarkers as potential therapeutic targets to improve treatment of stroke and management of post-stroke recovery. One recent DTI study demonstrated that a 6-month exercise-based cardiac rehabilitation program could reverse some of the cardiovascular disease-related WM microstructural alterations observed in ischemic heart disease patients following a cardiac event [33]. Likewise, this cardiac rehabilitation regimen could also be adapted to patients after stroke or transient ischemic attack [50]. These findings motivate the need for exploring WM therapies aimed at mitigating post-stroke WM degeneration and reducing risk of recurrent stroke, especially in patients with pre-existing WM disease. Anti-inflammatory treatment, if administered within an optimal therapeutic window, could aid this effort by quelling chronic pro-neuroinflammatory responses and may have favourable neuroplastic effects on cerebral WM recovery and cognitive outcomes in the months following ischemic stroke.

This study has a few limitations. PET and MRI data were acquired on a single-vendor PET/MRI scanner in a relatively small cohort, and a reference [^{18}F]FEPPA-PET was not performed at an earlier timepoint after the index stroke. The exclusion of patients with low-affinity TSPO binding– although necessary to minimize effects on TSPO-PET– contributed to the small sample size. The [^{18}F]FEPPA-PET findings were also limited by the lack of an available healthy control group matched in age and TSPO genotype to the stroke cohort. Future [^{18}F]FEPPA-PET studies with larger stroke cohorts and suitable healthy controls could be used to further explore neuroinflammatory loads after ischemic stroke and may

help distinguish post-stroke WM inflammation from normal age-related TSPO expression. Furthermore, the requirements for participation in this study implied a selection bias towards patients with minor physical and neuropsychological impairment from the stroke. In conjunction with the inclusion criterion of lack of substantial cognitive decline in the subjects' history, the MoCA scores were unsurprisingly in the higher range, indicating healthy cognitive status or, at worst, borderline MCI. Hence, this study was focused on assessment of changes in brain structure, rather than cognitive outcomes, following ischemic stroke. Patient outcome was not assessed in this cohort, therefore no conclusions can be drawn from this study regarding the potential clinical value of hybrid [^{18}F]FEPPA-PET/MRI in management of stroke and post-stroke cognitive outcomes.

The use of TSPO-PET to image neuroinflammation also has some limitations. Although TSPO is highly expressed in activated glia (microglia and astrocytes) during neuroinflammatory response to tissue damage, TSPO can also be taken up by peripheral macrophages as well as non-inflammatory cells involved in cerebrovascular function (i.e., endothelial cells, vascular smooth muscle cells) [13, 51–54]. However, to date, efforts to find a non-TSPO PET tracer that has superior performance for targeting glial activation have largely proven challenging [55, 56]. As such, TSPO-PET remains the current state-of-the-art choice for neuroinflammation imaging. Nevertheless, this study has piloted a clinically feasible PET/MR imaging approach to assess relationships between imaging biomarkers of post-acute WM degeneration following stroke. These findings motivate PET/MRI studies in larger cohorts, including advanced WM lesion quantification and assessments targeting specific cognitive domains to further investigate the associations between chronic neuroinflammation, ischemic WM injury, and post-stroke cognitive impairment.

Conclusions

In conclusion, this PET/MRI study demonstrated the utility of combining [^{18}F]FEPPA-PET, DTI, and FLAIR in probing post-acute changes in regional WM pathways in brains of elderly adults at 6-months following an acute ischemic stroke. Hybrid [^{18}F]FEPPA-PET/MRI revealed an association between elevations in post-acute glial activation (neuroinflammation) and reductions in microstructure integrity of brain WM pathways ipsilateral to ischemic infarcts and remote from WM lesions at 6-months post-stroke. Hybrid PET/MRI may help identify WM imaging biomarkers, such as chronic neuroinflammatory load and microstructural integrity, as potential therapeutic targets to mitigate post-acute WM degeneration and improve cognitive outcomes following ischemic stroke.

Abbreviations

AD	Axial diffusivity
AF	Arcuate fasciculus
ANTs	Advanced Normalization Tools
ATR	Anterior thalamic radiation
CAT	Computational Anatomy Toolbox
CC	Corpus callosum
CT	Computed tomography
DTI	Diffusion tensor imaging
DWI	Diffusion-weighted imaging
EPI	Echo-planar imaging
FA	Fractional anisotropy
FLAIR	Fluid attenuated inversion recovery
FSL	Functional MRI of the Brain Software Library
IQCODE	Informant Questionnaire on Cognitive Decline in the Elderly
MCI	Mild cognitive impairment
MD	Mean diffusivity
MNI	Montreal Neurological Institute
MoCA	Montreal Cognitive Assessment
MPRAGE	Magnetization-prepared rapid gradient-echo
MRI	Magnetic resonance imaging
NAWM	Normal appearing WM
NIHSS	National Institutes of Health Stroke Scale
NINDS-CSN	National Institute of Neurological Disorders and Stroke-Canadian Stroke Network
PET	Positron emission tomography
RD	Radial diffusivity
SLF	Superior longitudinal fasciculus
SPECT	Single-photon emission computed tomography
SPM	Statistical Parametric Mapping
SUV	Standardized uptake value
SUVr	SUV ratio
TSPO	Translocator protein
WM	White matter
WMH	WM hyperintensity

Acknowledgements

The authors thank Professor Wolf-Dieter Heiss for supporting data collection through funding from the Rolf M. Shwiete Stiftung trust at the Max Planck Institute for Metabolism Research, Cologne, Germany.

Author contributions

Conceived and designed the study: AVK and UCA. Patient recruitment and PET/MRI data collection: AVK and UCA. Clinical data collection: AVK and UCA. Created manual lesion segmentations: SEP, RW, PO, MTJ and AVK. Analyzed data: SEP, RW, LL, JDT, AVK and UCA. Interpreted data: SEP, RW, LL, PO, MTJ, AT, JDT, AVK and UCA. Manuscript preparation: SEP, JDT, AVK and UCA. All authors read and approved the final manuscript.

Funding

This work was supported by funding from the Heart and Stroke Foundation of Canada Grants-in-Aid Award (U.C.A., G-20-0029408), Lawson Health Research Institute Internal Research Fund (U.C.A., IRF-15-20), Canadian Institutes of Health Research (CIHR) Operating Grant: Joint Programme on Neurodegenerative Disease Research (U.C.A., 173743), CIHR Frederick and Charles Best Canada Graduate Scholarships Doctoral Award (S.E.P., FBD-181429), and the Max Planck Institute for Metabolism Research, Cologne, FR Germany, by a grant from the Rolf M. Shwiete Stiftung (A.V.K.).

Data availability

Data are available from the corresponding authors upon reasonable request and with permission of the Lawson Health Research Institute and Western University Research Ethics Board.

Declarations

Ethics approval and consent to participate

The study was approved by the Western University Research Ethics Board and conducted in accordance with the Declaration of Helsinki ethical standards. All patients provided written informed consent to participate.

Consent for publication
All patients gave written consent for publication.

Competing interests
All authors declare that they have no competing interests.

Author details
[1]Lawson Health Research Institute, London, ON, Canada
[2]Department of Medical Biophysics, Schulich School of Medicine and Dentistry, Western University, London, ON, Canada
[3]School of Medicine, Queen's University, Kingston, ON, Canada
[4]Department of Medical Imaging, Schulich School of Medicine and Dentistry, Western University, London, ON, Canada
[5]Department of Neurology and Neurosurgery, Jewish General Hospital, McGill University, Montréal, QC, Canada
[6]Division of Medical Physics, CancerCare Manitoba, Winnipeg, MB, Canada
[7]Department of Radiology, University of Manitoba, Winnipeg, MB, Canada
[8]Department of Clinical Neurological Sciences, Schulich School of Medicine and Dentistry, Western University, London, ON, Canada
[9]Department of Neurology and Neurosurgery, Montreal Neurological Institute, McGill University, Montréal, QC, Canada

Received: 12 February 2025 / Accepted: 10 July 2025
Published online: 23 July 2025

References

1. Cho A-H, Kim H-R, Kim W, Yang DW. White matter hyperintensity in ischemic stroke patients: It may regress over time. J Stroke. 2015;17:60–6.
2. Thiel A, Vahdat S. Structural and resting-state brain connectivity of motor networks after stroke. Stroke. 2015;46:296–301.
3. Kancheva I, Buma F, Kwakkel G, Kancheva A, Ramsey N, Raemaekers M. Investigating secondary white matter degeneration following ischemic stroke by modelling affected fiber tracts. NeuroImage: Clin. 2022;33:102945.
4. Bonkhoff AK, Hong S, Bretzner M, Schirmer MD, Regenhardt RW, Arsava EM, et al. Association of stroke lesion pattern and white matter hyperintensity burden with stroke severity and outcome. Neurology. 2022;99:e1364–79.
5. de Groot M, Verhaaren BFJ, de Boer R, Klein S, Hofman A, van der Lugt A, et al. Changes in normal-appearing white matter precede development of white matter lesions. Stroke. 2013;44:1037–42.
6. Egorova-Brumley N, Dhollander T, Khan W, Khlif MS, Ebaid D, Brodtmann A. Changes in white matter microstructure over 3 years in people with and without stroke. Neurology. 2023;100:e1664–72.
7. Thiel A, Radlinska BA, Paquette C, Sidel M, Soucy J-P, Schirrmacher R, et al. The temporal dynamics of poststroke neuroinflammation: A longitudinal diffusion tensor imaging–guided PET study with 11C-PK11195 in acute subcortical stroke. J Nucl Med. 2010;51:1404–12.
8. Thiel A, Heiss W-D. Imaging of microglia activation in stroke. Stroke. 2011;42:507–12.
9. Candelario-Jalil E, Dijkhuizen RM, Magnus T. Neuroinflammation, stroke, blood-brain barrier dysfunction, and imaging modalities. Stroke. 2022;53:1473–86.
10. Fan Z, Brooks DJ, Okello A, Edison P. An early and late peak in microglial activation in Alzheimer's disease trajectory. Brain. 2017;140:792–803.
11. Thackeray JT. Imaging the molecular footprints of the heart–brain axis in cardiovascular disease. J Nucl Med. 2019;60:728–9.
12. Thiel A, Cechetto DF, Heiss W-D, Hachinski V, Whitehead SN. Amyloid burden, neuroinflammation, and links to cognitive decline after ischemic stroke. Stroke. 2014;45:2825–9.
13. Van Camp N, Lavisse S, Roost P, Gubinelli F, Hillmer A, Boutin H. TSPO imaging in animal models of brain diseases. Eur J Nucl Med Mol Imaging. 2021;49:77–109.
14. Tang JM, McClennan A, Liu L, Hadway J, Ronald JA, Hicks JW, et al. A protocol for simultaneous in vivo imaging of cardiac and neuroinflammation in dystrophin-deficient MDX mice using [18F]FEPPA PET. Int J Mol Sci. 2023;24:7522.
15. Kreisl WC, Lyoo CH, McGwier M, Snow J, Jenko KJ, Kimura N, et al. In vivo radioligand binding to translocator protein correlates with severity of Alzheimer's disease. Brain. 2013;136:2228–38.
16. Lavisse S, Goutal S, Wimberley C, Tonietto M, Bottlaender M, Gervais P, et al. Increased microglial activation in patients with Parkinson disease using [18F]-DPA714 TSPO PET imaging. Parkinsonism Relat Disord. 2021;82:29–36.
17. Pascual B, Funk Q, Zanotti-Fregonara P, Cykowski MD, Veronese M, Rockers E, et al. Neuroinflammation is highest in areas of disease progression in semantic dementia. Brain. 2021;144:1565–75.
18. Cakmak JD, Liu L, Poirier SE, Schaefer B, Poolacherla R, Burhan AM, et al. The functional and structural associations of aberrant microglial activity in major depressive disorder. J Psychiatry Neurosci. 2022;47:E197–208.
19. Viviano M, Barresi E, Siméon FG, Costa B, Taliani S, Da Settimo F, et al. Essential principles and recent progress in the development of TSPO PET ligands for neuroinflammation imaging. Curr Med Chem. 2022;29:4862–90.
20. Ribeiro M-J, Vercouillie J, Debiais S, Cottier J-P, Bonnaud I, Camus V, et al. Could 18 F-DPA-714 PET imaging be interesting to use in the early post-stroke period? EJNMMI Res. 2014;4:28.
21. Suridjan I, Pollock BG, Verhoeff NPLG, Voineskos AN, Chow T, Rusjan PM, et al. In-vivo imaging of grey and white matter neuroinflammation in Alzheimer's disease: a positron emission tomography study with a novel radioligand, [18 F]-FEPPA. Mol Psychiatry. 2015;20:1579–87.
22. Al-Khishman NU, Qi Q, Roseborough AD, Levit A, Allman BL, Anazodo UC, et al. TSPO PET detects acute neuroinflammation but not diffuse chronically activated MHCII microglia in the rat. EJNMMI Res. 2020;10:113.
23. Owen DR, Yeo AJ, Gunn RN, Song K, Wadsworth G, Lewis A, et al. An 18-kDa translocator protein (TSPO) polymorphism explains differences in binding affinity of the PET radioligand PBR28. J Cereb Blood Flow Metab. 2012;32:1–5.
24. Nasreddine ZS, Phillips NA, Bédirian V, Charbonneau S, Whitehead V, Collin I, et al. The Montreal Cognitive Assessment, MoCA: A brief screening tool for mild cognitive impairment. J Am Geriatr Soc. 2005;53:695–9.
25. Izquierdo-Garcia D, Hansen AE, Förster S, Benoit D, Schachoff S, Fürst S, et al. An SPM8-based approach for attenuation correction combining segmentation and non-rigid template formation: Application to simultaneous PET/MR brain imaging. J Nucl Med. 2014;55:1825–30.
26. Woolrich MW, Jbabdi S, Patenaude B, Chappell M, Makni S, Behrens T, et al. Bayesian analysis of neuroimaging data in FSL. NeuroImage. 2009;45:S173–86.
27. Gaser C, Dahnke R, Thompson PM, Kurth F, Luders E, the Alzheimer's Disease Neuroimaging Initiative. CAT: a computational anatomy toolbox for the analysis of structural MRI data. GigaScience. 2024;13:giae049.
28. Yushkevich PA, Piven J, Hazlett HC, Smith RG, Ho S, Gee JC, et al. User-guided 3D active contour segmentation of anatomical structures: Significantly improved efficiency and reliability. NeuroImage. 2006;31:1116–28.
29. Avants BB, Tustison NJ, Song G, Cook PA, Klein A, Gee JC. A reproducible evaluation of ANTs similarity metric performance in brain image registration. NeuroImage. 2011;54:2033–44.
30. Lyoo CH, Ikawa M, Liow J-S, Zoghbi SS, Morse CL, Pike VW, et al. Cerebellum can serve as a pseudo-reference region in Alzheimer disease to detect neuroinflammation measured with PET radioligand binding to translocator protein. J Nucl Med. 2015;56:701–6.
31. Poirier SE, Kwan BYM, Jurkiewicz MT, Samargandy L, Steven DA, Suller-Marti A, et al. 18F-FDG PET-guided diffusion tractography reveals white matter abnormalities around the epileptic focus in medically refractory epilepsy: implications for epilepsy surgical evaluation. Eur J Hybrid Imaging. 2020;4:10.
32. Wasserthal J, Neher P, Maier-Hein KH. TractSeg - Fast and accurate white matter tract segmentation. NeuroImage. 2018;183:239–53.
33. Poirier SE, Suskin NG, Khaw AV, Thiessen JD, Shoemaker JK, Anazodo UC. Probing evidence of cerebral white matter microstructural disruptions in ischemic heart disease before and following cardiac rehabilitation: A diffusion tensor MR imaging study. J Magn Reson Imaging. 2024;59:2137–49.
34. Vermeer SE, Hollander M, van Dijk EJ, Hofman A, Koudstaal PJ, Breteler MMB. Silent brain infarcts and white matter lesions increase stroke risk in the general population. Stroke. 2003;34:1126–9.
35. Feng W, Wang J, Chhatbar PY, Doughty C, Landsittel D, Lioutas V-A, et al. Corticospinal tract lesion load: An imaging biomarker for stroke motor outcomes. Ann Neurol. 2015;78:860–70.
36. Puig J, Blasco G, Daunis-I-Estadella J, Thomalla G, Castellanos M, Figueras J, et al. Decreased corticospinal tract fractional anisotropy predicts long-term motor outcome after stroke. Stroke. 2013;44:2016–8.
37. DiBella EVR, Sharma A, Richards L, Prabhakaran V, Majersik JJ, Hashemizadeh-Kolowri SK. Beyond diffusion tensor MRI methods for improved characterization of the brain after ischemic stroke: A review. Am J Neuroradiol. 2022;43:661–9.
38. Stuckey SM, Ong LK, Collins-Praino LE, Turner RJ. Neuroinflammation as a key driver of secondary neurodegeneration following stroke? Int J Mol Sci. 2021;22:13101.

39. Radlinska BA, Ghinani SA, Lyon P, Jolly D, Soucy J-P, Minuk J, et al. Multimodal microglia imaging of fiber tracts in acute subcortical stroke. Ann Neurol. 2009;66:825–32.
40. Owen DR, Narayan N, Wells L, Healy L, Smyth E, Rabiner EA, et al. Pro-inflammatory activation of primary microglia and macrophages increases 18 kDa translocator protein expression in rodents but not humans. J Cereb Blood Flow Metab. 2017;37:2679–90.
41. Schaechter JD, Hightower BG, Kim M, Loggia ML. A pilot [11C]PBR28 PET/MRI study of neuroinflammation and neurodegeneration in chronic stroke patients. Brain Behav Immun Health. 2021;17:100336.
42. Jensen P, Ozenne B, Meden P, Feng L, Thomsen G, Knudsen L, et al. Poststroke translocator protein expression dynamics and correlations to chronic infarction: A [123I]-CLINDE-SPECT study. J Neuroimaging. 2025;35:e70002.
43. Anazodo UC, Wong DY, Théberge J, Dacey M, Gomes J, Penny JD, et al. Hemodialysis-related acute brain injury demonstrated by application of intradialytic magnetic resonance imaging and spectroscopy. J Am Soc Nephrol. 2023;34:1090.
44. Basilakos A, Fillmore PT, Rorden C, Guo D, Bonilha L, Fridriksson J. Regional white matter damage predicts speech fluency in chronic post-stroke aphasia. Front Hum Neurosci. 2014;8:845.
45. Urbanski M, Thiebaut de Schotten M, Rodrigo S, Oppenheim C, Touzé E, Méder J-F, et al. DTI-MR tractography of white matter damage in stroke patients with neglect. Exp Brain Res. 2011;208:491–505.
46. Malek-Ahmadi M, Nikkhahmanesh N. Meta-analysis of Montreal cognitive assessment diagnostic accuracy in amnestic mild cognitive impairment. Front Psychol. 2024;15:1369766.
47. Zaidi K-B, Rich JB, Sunderland KM, Binns MA, Truong L, McLaughlin PM, et al. Methods for improving screening for vascular cognitive impairment using the Montreal Cognitive Assessment. Can J Neurol Sci. 2020;47:756–63.
48. Hachinski V, Iadecola C, Petersen RC, Breteler MM, Nyenhuis DL, Black SE, et al. National Institute of Neurological Disorders and Stroke–Canadian Stroke Network vascular cognitive impairment harmonization standards. Stroke. 2006;37:2220–41.
49. Thienel R, Borne L, Faucher C, Behler A, Robinson GA, Fripp J, et al. Can an online battery match in-person cognitive testing in providing information about age-related cortical morphology? Brain Imaging Behav. 2024;18:1215–25.
50. Prior PL, Hachinski V, Chan R, Unsworth K, Mytka S, Harnadek M, et al. Comprehensive cardiac rehabilitation for secondary prevention after transient ischemic attack or mild stroke: PSYCHOLOGICAL PROFILE AND OUTCOMES. J Cardiopulm Rehabil Prev. 2017;37:428–36.
51. Nutma E, Ceyzériat K, Amor S, Tsartsalis S, Millet P, Owen DR, et al. Cellular sources of TSPO expression in healthy and diseased brain. Eur J Nucl Med Mol Imaging. 2021;49:146–63.
52. Gui Y, Marks JD, Das S, Hyman BT, Serrano-Pozo A. Characterization of the 18 kDa translocator protein (TSPO) expression in post-mortem normal and Alzheimer's disease brains. Brain Pathol. 2020;30:151–64.
53. Ceyzériat K, Nicolaides A, Amossé Q, Fossey C, Cailly T, Fabis F, et al. Reactive astrocytes mediate TSPO overexpression in response to sustained CNTF exposure in the rat striatum. Mol Brain. 2023;16:57.
54. Wijesinghe SS, Rowe JB, Mason HD, Allinson KSJ, Thomas R, Vontobel DS, et al. Post-mortem validation of in vivo TSPO PET as a microglial biomarker. Brain. 2025;148:1904–10.
55. Chauveau F, Winkeler A, Chalon S, Boutin H, Becker G. PET imaging of neuroinflammation: any credible alternatives to TSPO yet? Mol Psychiatry. 2025;30:213–28.
56. Nutma E, Fancy N, Weinert M, Tsartsalis S, Marzin MC, Muirhead RCJ, et al. Translocator protein is a marker of activated microglia in rodent models but not human neurodegenerative diseases. Nat Commun. 2023;14:5247.

Publisher's note